2018

Feasibility of co-registered ultrasound and acoustic-resolution photoacoustic imaging of human colorectal cancer

Xiandong Leng
Washington University in St. Louis

William Chapman
Washington University School of Medicine in St. Louis

Bin Rao
Washington University in St. Louis

Sreyankar Nandy
Washington University in St. Louis

Ruimin Chen
University of Southern California

See next page for additional authors

Authors
Xiandong Leng, William Chapman, Bin Rao, Sreyankar Nandy, Ruimin Chen, Rehan Rais, Ivan Gonzalez, Qifa Zhou, Deyali Chatterjee, Matthew Mutch, and Quing Zhu

Research Article | Vol. 9, No. 11 | 1 Nov 2018 | BIOMEDICAL OPTICS EXPRESS 5159
Biomedical Optics EXPRESS

Feasibility of co-registered ultrasound and acoustic-resolution photoacoustic imaging of human colorectal cancer

XIANDONG LENG,[1] WILLIAM CHAPMAN JR.,[2] BIN RAO,[1,3] SREYANKAR NANDY,[1] RUIMIN CHEN,[4] REHAN RAIS,[5] IVAN GONZALEZ,[5] QIFA ZHOU,[4,6] DEYALI CHATTERJEE[5] MATTHEW MUTCH,[2] AND QUING ZHU[1,7,*]

[1]*Department of Biomedical Engineering, Washington University in St. Louis, St. Louis, MO 63130, USA*
[2]*Division of Surgery, Banes-Jewish Hospital, Washington University in St. Louis, St. Louis, MO 63130, USA*
[3]*Applied Bioptics LLC, St. Louis, 63146, MO, USA*
[4]*Department of Biomedical Engineering, University of Southern California, Los Angeles, CA 90007, USA*
[5]*Department of Pathology and Immunology, Washington University School of Medicine, St. Louis, MO 63110, USA*
[6]*Department of Ophthalmology, University of Southern California, Los Angeles, CA 90007, US*
[7]*Department of Radiology, Washington University School of Medicine, St. Louis, MO 63110, USA*
**zhu.q@wustl.edu*

Abstract: Colorectal cancer is the second leading cause of cancer death in the United States. Significant limitations in screening and surveillance modalities continue to hamper early detection of primary cancers or recurrences after therapy. In this study, we describe a new registered ultrasound (US) and acoustic-resolution photoacoustic microscopy (AR-PAM) system and report its initial testing in *ex vivo* human colorectal tissue. A total of 8 colorectal specimens were imaged, which included 2 polyps, 4 malignant colon cancers, and 2 treated colorectal cancers. In each specimen, normal tissue was also imaged for internal control. Initial data have demonstrated the feasibility of identifying colorectal cancer imaging features and the invasion depth using co-registered US and an AR-PAM system. In normal tissue, we found that our system consistently demonstrates the multi-layer structure of normal colonic tissue while differentiating layers with elevated vascularity; these findings highly correlated with histologic findings of each specimen. For malignant colorectal samples, the tissue structure is highly disorganized as seen in US, and photoacoustic imaging revealed distorted vascular distribution inside the tumor. Notably, AR-PAM of tumor beds after complete tumor destruction by radiation and chemotherapy yielded a pattern identical to benign tissue. Quantitative analysis of photoacoustic spectral slope has demonstrated more high-frequency components in malignant tissue as compared to the normal colon tissue, which may be caused by significantly increased microvessel networks. In summary, we demonstrate the successful differentiation of benign and malignant colorectal tissue with our co-registered ultrasound and photoacoustic system.

1. Introduction

Photoacoustic imaging (PAI) techniques have demonstrated a unique ability to resolve optical absorption contrast in biological tissues [1,2], which can be invaluable for detection and diagnosis of tumor microvasculature or tumor angiogenesis [3,4]. PAI technique is based on the photoacoustic principle: as pulsed laser is delivered to tissue, photon energy absorbed by biomolecules converts to heat and creates an initial pressure wave [5]. This wave is detectable by an ultrasonic transducer. In tissue, PAI transforms hemoglobin into an endogenous

#342357 https://doi.org/10.1364/BOE.9.005159
Journal © 2018 Received 15 Aug 2018; revised 24 Sep 2018; accepted 25 Sep 2018; published 3 Oct 2018

Biomedical Optics EXPRESS

contrast agent that can be used to determine various functional and anatomic characteristics not available with basic endoscopy.

In general, photoacoustic microscopy (PAM) is classified into optical-resolution (OR) PAM and acoustic-resolution (AR) PAM [6]; AR-PAM is able to penetrate deeper than OR-PAM due to the use of acoustic focusing rather than optical focusing through tissue. Previous groups have applied this technology to image the esophagus and gastrointestinal tract of small animals, but no prior applications in the human distal GI tract have been described [7] [8]. Clinically, PAI has the potential to detect, in real time, both anatomic and functional changes that are otherwise not captured by traditional radiographic techniques.

Photoacoustic spectrum analysis (PASA) is a powerful tool to quantify and characterize tissue microstructural changes. Strohm et al has demonstrated distinct features of red blood cell (RBC) morphology and tissue architecture in photoacoustic spectrum [9]. Xu et al has shown that photoacoustic spectrum parameters of spectral intercept, midband-fit, and spectral slope can differentiate normal and fatty mouse livers [10]. Chitnis et al has systematically evaluated photoacoustic spectral intercept, spectral slope, and effective-absorber size in differentiating tissue constituents [11]. Our group has shown that photoacoustic and ultrasound spectral parameters can be used to characterize malignant and benign/normal ovarian tissues [12,13].

Colorectal adenocarcinoma is a common cancer with an estimated annual incidence of over 100,000 cases in the United States [14]. Though white light endoscopy and pelvic magnetic resonance imaging (MRI) are the current gold standard techniques for detecting and surveilling these tumors, both modalities have significant shortcomings. Endoscopy only detects abnormalities of the mucosal surface of the colon and provides no assessment of oncologic activity in deeper aspects of the bowel. Yet MRI, which provides cross-sectional imaging of the entire pelvis, cannot achieve a resolution less than 1.5cm, limiting its ability to evaluate the GI tract for small malignancies or abnormalities. Additionally, MRI is not specific for evaluating post-treatment cancers due to inability to distinguish viable tumor from residual scar and fibrous tissue [15]. This shortcoming, in particular, currently limits widespread utilization of a promising new treatment option in rectal cancer that avoids surgical intervention altogether. Therefore, there exists an urgent need for new modalities that allow high resolution evaluation of the colorectum at all levels.

In this study, we report the development and initial clinical testing of an AR-PAM system suitable for human colorectal cancer imaging. We hypothesized that AR-PAM would provide new insight into both colonic and rectal morphology in the setting of both untreated and treated tumors. We utilized phantoms and freshly excised human colon and rectal tissue to test parameters of the AR-PAM system and examine imaging patterns in human tissue. We also developed a novel comparative mechanism using PAM spectral slopes to quantify differences between malignant and benign tissue.

2. Materials and methods

2.1 Design and construction of the AR-PAM system

Our endoscopic AR-PAM design is shown in Fig. 1(a)-(c). A multi-mode fiber (1.5mm diameter, numerical aperture of 0.39) delivers 750nm laser pulse to the imaging head. At the distal end of the imaging head, a focused ring transducer (4.0mm O.D., f = 12.7mm, 20MHz) is installed on the side; a 45° rod mirror reflects the laser beam 90° to tissue surface through a center hole of the ring transducer. 10mJ laser pulse illuminates a tissue area of 0.6 cm^2; surface optical influence is 16.7mJ/cm^2, which is within safety standards [16].

Biomedical Optics EXPRESS

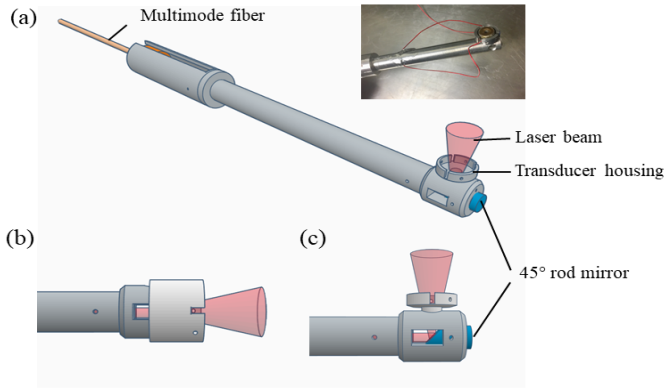

Fig. 1. (a)AR-PAM imaging head, (b) forward imaging mode, (c) side-view image mode.

Figure 1(a) inset shows a photograph of the AR-PAM imaging head. Figure 1(b) and 1(c) show the forward view and side view modes of the AR-PAM, respectively; forward view facilitates bench-top scanning while sideview mode is suitable for endoscope use. Forward view mode is used in this study.

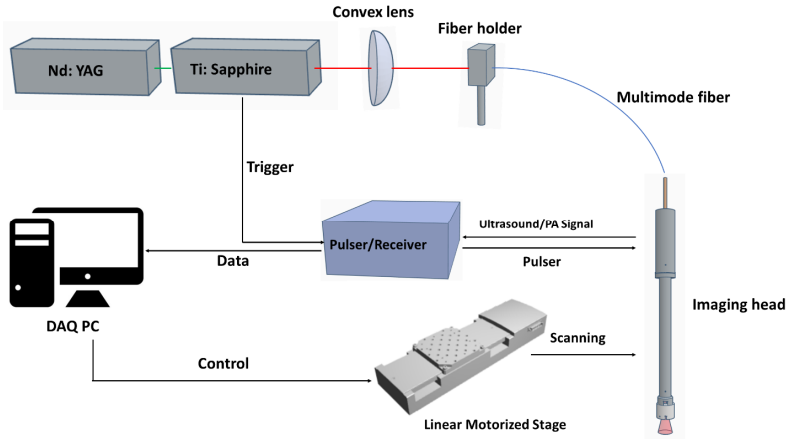

Fig. 2. AR-PAM system.

The complete system is shown in Fig. 2. Light output from a Nd:YAG (Lotis TII) pumped Ti:Sapphire (15 Hz, 10 ns) laser tunable from 700 nm to 900 nm is focused by a convex lens (f = 40mm) to a multi-mode fiber. Distal end of multimode fiber is fixed on the endoscopic AR-PAM. A pulser/receiver (Panametrics 5900PR) is used to amplify photoacoustic signal in PA mode and obtain ultrasound image in Pulse/Echo mode. Sequentially co-registered photoacoustic and ultrasound data are acquired by a DAQ card. Motor scanning is controlled through an analog output card (National Instrument PCI 6251). This system takes 7 seconds to finish an ultrasound B-scan and 56 seconds for a photoacoustic B-scan of 20mm. Scanning speed is limited by the 15 Hz laser system.

2.2 Performance testing

Initial calibration and testing of the AR-PAM system involved three steps. First, we performed Fourier transformation of the ultrasound echo from glass into water to determine ring transducer frequency. Second, we evaluated the lateral and axial resolution of the AR-PAM system by imaging a 7µm diameter carbon fiber. The ultrasonic transducer focal point is placed in the carbon fiber horizontal plane and cross-sectional images of the carbon fiber were obtained. Axial and lateral resolution were then calculated based on these tests. Finally,

Biomedical Optics EXPRESS

we tested the signal-to-noise ratio (SNR) at different target depths using a black cotton string in 0.4% intralipid solution. Starting at the level of the transducer, the distance between the transducer lens and the black string was increased by increments of 0.5mm. Photoacoustic A-scan images were then used to calculate the SNR.

2.3 Human colorectal samples

After system testing and calibration was performed, we conducted a pilot study of *ex vivo* human colorectal specimens to evaluate tissue characteristics under AR-PAM imaging. Specimens were collected from consenting patients undergoing colon or rectal resection of a known neoplastic lesion at Washington University School of Medicine. This study was approved by the Institutional Review Board (IRB) at Washington University. Each specimen was evaluated prior to formalin fixation to preclude tissue architectural alteration. To protect the specimens from excessive breakdown prior to histologic evaluation, all the imaging was completed within one hour of surgery. Specimens were then fixed in formalin and processed under normal staining and sectioning protocols. Hematoxylin and eosin (H&E) staining was performed on all specimens. Additional immunohistochemistry was performed with CD31 antibodies to highlight vascular structures on select specimens for correlation of vascular histology with photoacoustic findings.

2.4 Data analysis

Data were analyzed both qualitatively and quantitatively. Qualitative analysis included comparison of AR-PAM generated images with histology; specific attention was paid to the layers of the tissue as well as the vascular organization of the tissues in question. To facilitate quantitative analysis, we utilized a measure of photoacoustic power spectral slope [12]. To calculate this parameter, power spectra were derived from fast Fourier transformation (FFT) on photoacoustic beams. Then, we performed linear fitting of the spectra in the range of transducer frequency responses. After the linear fitting, spectral slopes of each imaged malignant and benign area were then plotted using boxplot; Student t-test was used to calculate the statistical significance between malignant and normal group, as well as polyps and normal group, and $p<0.05$ was considered significant.

3. Results

3.1 AR-PAM calibration and testing

Initial device performance testing demonstrated consistent characteristics across multiple tests (Fig. 3). Lateral and axial resolution were found to be 65µm and 45µm, respectively. In 0.4% intralipid solution (with an approximate 4 cm^{-1} reduced scattering coefficient), the signal-to-noise ratio (SNR) varied from 42dB at 0.5mm to 18dB at 4.5mm.

Biomedical Optics EXPRESS

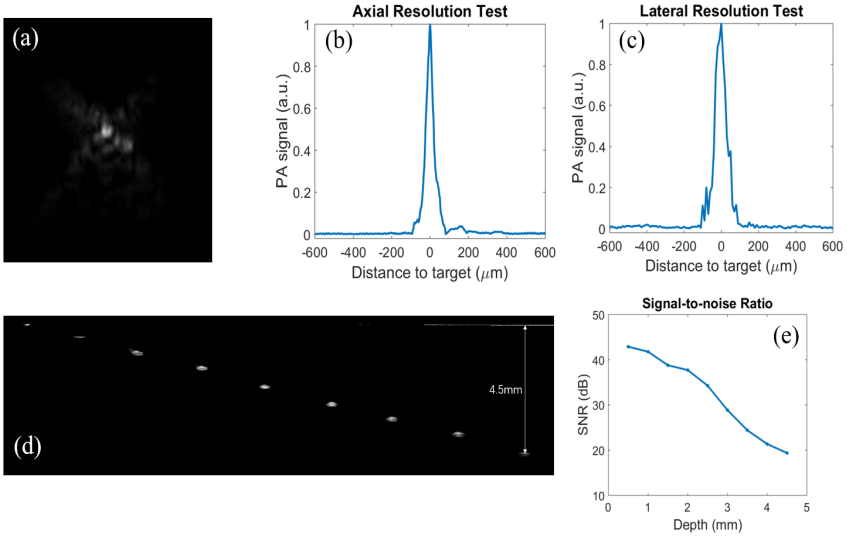

Fig. 3. (a) cross-sectional image of 7µm carbon fiber, (b) lateral resolution, (c) axial resolution, (d) depth test in intralipid, (e) SNR versus target depth

3.2 Ex vivo sample imaging - qualitative analysis

Eight specimens were imaged during this pilot study which included cancer without prior treatment, neoplastic polyps without malignancy, colon cancer after chemotherapy, and rectal cancer after radiation and chemotherapy (Table 1). Average imaging time of a 20mm cross sectional area of bowel was 1 minute. No system malfunctions or tissue damage occurred throughout the pilot study.

Table 1. Summary of Specimen

Case number	Surgery	Pathologic result	Treatment method
1	Sigmoid colectomy	Adenomatous polyp with focus of adenocarcinoma	N/A
2	Right hemicolectomy	T2N0 moderately differentiated adenocarcinoma	N/A
3	Sigmoid colectomy	T3N1 adenocarcinoma	Chemotherapy
4	Low anterior resection	Complete pathologic response - no residual tumor	Radiotherapy and chemotherapy
5	Sigmoid colectomy	T3N0 adenocarcinoma	N/A
6	Total colectomy	T3N1 adenocarcinoma	N/A
7	Right hemicolectomy	Tubular adenoma	N/A
8	Right hemicolectomy	Tubular adenoma	N/A

3.2.1. Colonic polyp

Figure 4 displays several representative images obtained with the AR-PAM system on a segment of bowel (case 1) that included a known adenomatous polyp; both the polyp and a grossly normal segment of bowel were imaged. Photographs of these imaged areas (Fig. 4(a) and 4(e)) were collected at time of imaging; the white arrows indicate the plane through which the corresponding cross-sectional imaging was collected.

Biomedical Optics EXPRESS

On ultrasound imaging alone, the normal layered structure of the colon wall appears to be clearly delineated (Fig. 4b). On the surface, the first two layers (L1 and L2) appear to represent the mucosal surface of the colon and likely includes the muscularis mucosa. Under the muscularis, the basement membrane (L3) appears echogenic (white) and overlies a thick hypoechoic layer (L4) corresponding to the submucosa. Finally, the deepest layer (approximately 1 mm from the endoluminal surface) is the muscularis propria (L5) and appears as the thickest layer.

Figure 4(c) shows the same ultrasound image now co-registered with photoacoustic signals, demonstrating areas of vascular signal within the segment of bowel. Heavy concentrations of blood vessels are noted within the submucosa (indicated by high intensity of color); note also the relative paucity of signal within the underlying muscle. H&E images from the same specimen correlate with the co-registered ultrasound and AR-PAM images – the submucosa is rich in vascular structures while the underlying muscle lacks organized vessels (Fig. 4(d)).

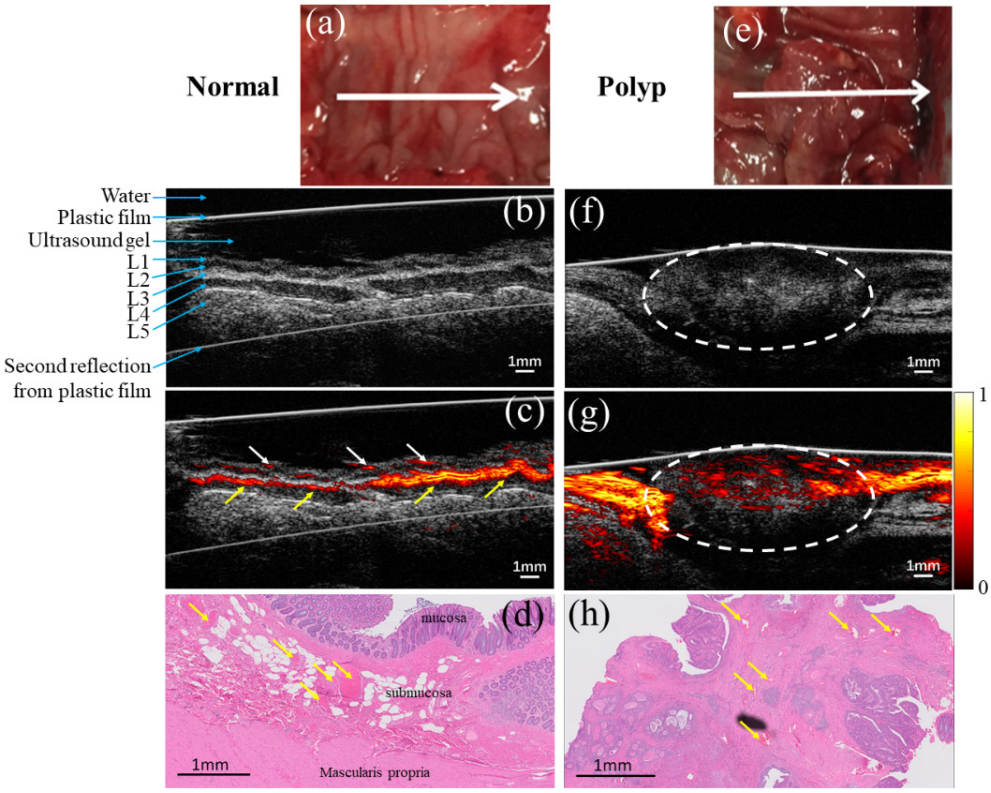

Fig. 4. Photograph of (a) normal colon and (e) adenomatous colon polyp; (b) ultrasound image of the normal tissue; (c) co-registered ultrasound and photoacoustic image of the same cross section of (b), white arrows refer to blood vessel in mucosa and yellow arrows refer to blood vessel in submucosa; (f) ultrasound image of polyp, tissue inside dashed line is polyp; (g) co-registered ultrasound and photoacoustic image of the same cross section of (f); (d) and (h) are H&E images of normal tissue and polyp, yellow arrows identify blood vessels.

Evaluation of the adenomatous polyp, however, shows two marked differences: loss of the organized layers seen in the normal colon and replacement with a peripherally vascularized but centrally quiescent, disorganized mass. In the standalone ultrasound image (Fig. 4(f)), the polyp (surrounded by dashed line) appears as an oval shape of disorganized tissue without distinguishable layers. On co-registered imaging, the photoacoustic signal pattern demonstrates loss of overall signal within the polyp (Fig. 4(g)). Note, however, the

Biomedical Optics EXPRESS

hyperintensity within the submucosa of the normal bowel surrounding the polyp (outside the dashed white line). The lack of organized vascularity within the polyp correlates well with histology; relatively few vessels are noted within the polypoid tissue itself (Fig. 4(h)). In contrast to the normal, layered structure with consistent vascularity in the submucosa, the abnormal polyp appears disorganized and hypovascular on imaging with the AR-PAM system. Interestingly, there is an increase in photoacoustic signal surrounding the polyp, suggesting a hypervascular response to the neoplastic tissue.

3.2.2. Colon cancer–no prior treatment

AR-PAM found similar findings among imaged colon malignancies. Upon evaluation of a colon cancer confined to the superficial layers of the colonic wall, AR-PAM again demonstrated loss of layered structure as well as intra-lesion hypovascularity compared to normal tissue. Figure 5 shows the imaging results from one representative colon cancer specimen, case 2.

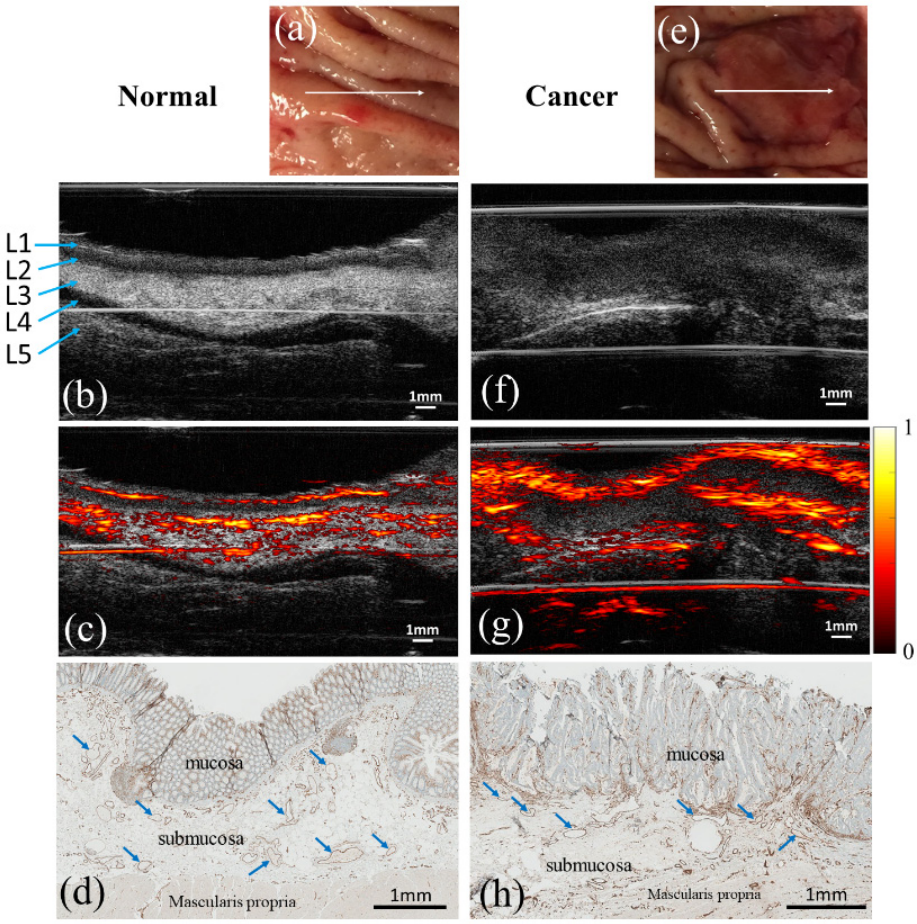

Fig. 5. Gross photographic, ultrasound, coregistered, and CD31-stained histologic images of Specimen 2. (a) Photograph of the normal tissue, (b) ultrasound image of the normal tissue, (c) co-registered ultrasound and photoacoustic image of (b). (e) Photograph of cancer area, (f) and (g) are ultrasound and co-registered image of cancer. (d) and (h) are CD31 images of normal and cancer tissue, respectively, blue arrows point to blood vessels.

Figure 5(f) and (g) correspond to ultrasound and co-registered images of the malignant lesion of this specimen. As in the polyp case, images of the normal bowel show consistent

Biomedical Optics EXPRESS

layering with concentration of the vascular structures in the submucosa (Fig. 5(b)(c)). In contrast, tumor imaging shows loss of the normal layering as well as hypointense signaling from within the mass. Unlike the polyp, the tumor demonstrated markedly increased photoacoustic signal peripheral to the tumor, particularly on the mucosal surface. Histologic evaluation with CD31 targeted immunohistochemistry confirms these findings; heavy uptake of brown stain by endothelial lined blood vessels is noted at the mucosal surface of the tumor but remains centrally located in the submucosa of the normal specimen.

3.2.3. Colon cancer–prior chemotherapy with residual disease

Case 3 included a colon cancer previously treated with six cycles of chemotherapy that completed twenty days prior to surgical resection (Fig. 6 a-d). Figure 6(a) is a photograph of the ulcerated tumor bed surrounded by normal-appearing mucosa. Similar to previous lesions, ultrasound imaging across the lesion center demonstrated a peripheral multilayer structure that became disorganized within the actual tumor bed (central portion of Fig. 6(b) beneath the gel-filled ulcer cavity). Similarly, the co-registered photoacoustic image (Fig. 6(c)) also demonstrated relatively normal findings in the periphery; however, the regular photoacoustic signal distribution pattern transformed into hyperintense areas of high signal immediately around and below the ulceration (findings similar to non-treated cancerous tissues). Corresponding to the photoacoustic findings, histologic evaluation yielded a significant amount of residual cancer around the ulcerated cavity (Fig. 6(d)). In essence, the photoacoustic signal pattern appears to correlate with the malignant tissue found in proximity to the ulcer cavity.

These images suggest that chemotherapy, in the absence of complete tumor death, does not reverse the alterations in AR-PAM signal noted in malignant tissue.

3.2.4. Rectal cancer–prior chemotherapy and radiation without residual disease

We also evaluated a rectal specimen (Case 4) with a known malignancy that had been treated with 2500 cGy of radiation and twelve cycles of chemotherapy before surgical resection (Fig. 7(a-d)). The radiation, administered in 5 daily fractions, concluded 243 days prior to surgical resection and imaging. Gross evaluation demonstrated a pale, firm scar but no signs of active cancer (Fig. 7(a)). Unlike the previously described cancer specimens, both ultrasound and photoacoustic images yield a regularly layered structure with normal vascular distribution in the submucosa (Fig. 7(b) and 7(c)). In fact, these images appear much more similar to the patterns noted in the normal tissue in cases 1 and 2. Subsequent histologic evaluation of the specimen revealed no viable cancer cells; instead, the preoperative radiation and chemotherapy had completely destroyed the malignancy. Only fibrous scar tissue and mucin pools delineated the area of prior cancer (Fig. 7(d)). Blood vessels, labeled by yellow arrows, were noted throughout the submucosa.

In other words, this specimen suggests that complete tumor death after treatment results in return of tissue to normal-appearing AR-PAM signal. Ultrasound detects standard layering of the bowel wall, and AR-PAM detects homogenous vascular signal within the submucosa-mirroring the findings of normal bowel. Significantly, scar tissue formed by the dead tumor does not appear to interfere with the return of normal vascular signal to these tissue areas. This may be a very significant finding, as it suggests a possible method for differentiating incomplete versus complete tumor responses.

3.3 Quantitative analysis

In addition to the qualitative comparisons reported above, we also used spectral slope to quantify differences between tissue types. Eight imaged areas – four neoplastic and four normal – were included in spectral slope calculations as described previously [12]. After deriving the center frequency of the transducer at 20 MHz with full width at half maximum (FWHM) from 12.5MHz to 27.5MHz, the linear fitting of spectrum in FWHM frequency

Biomedical Optics EXPRESS

range was found in each specimen. Figures 8(c) and 8(e) demonstrate the range of PA signal from normal and cancer areas, respectively. Likewise, Figs. 8(d) and 8(f) show the power spectrum of signals demonstrated in 8(c) and 8(e). These power spectra were then combined to calculate a slope among all the cancer and all the normal tissues. For tumors, the median value of spectral slope (absolute value) of malignant group is significantly lower than that of normal tissue (0.9376 vs. 1.2551, respectively; $p<0.01$; Fig. 8(g) and Table 2). Table 2 displays spectral slopes for each of the eight imaged areas previously described. Note that for boxplot Fig. 8(g), 4 cancer cases, 4 normal cases, 2 polyp cases, 1 treated rectal cancer case, and 1 residual of colon cancer case are included. Among them, 4 normal tissues are from non-cancer normal areas of specimens with cancer.

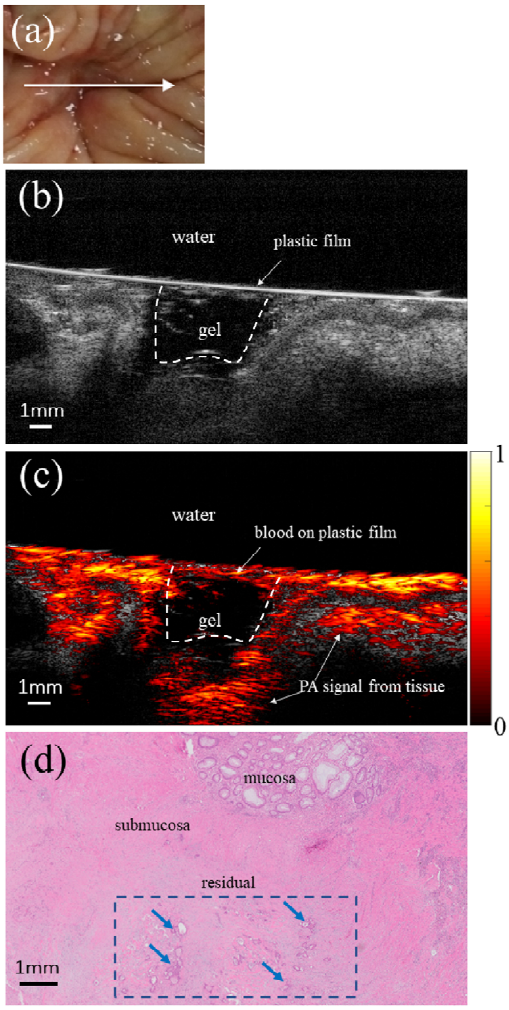

Fig. 6. Images obtained from select areas of Specimen 3 – a colon cancer treated with chemotherapy prior to resection. (a) Photograph of the post treated colon tumor area demonstrating a contracted, scarred ulcer, (b) ultrasound image of the lesion (note that ultrasound gel fills the ulcer cavity (dashed line) but is not within the tissue) (c) co-registered ultrasound and photoacoustic image demonstrating increased photoacoustic signal around the ulcerated area; (d) H&E image of the tumor bed showing residual islands of cancer cells (blue arrows within the dashed box) several millimeters beneath the surface of the specimen.

Biomedical Optics EXPRESS

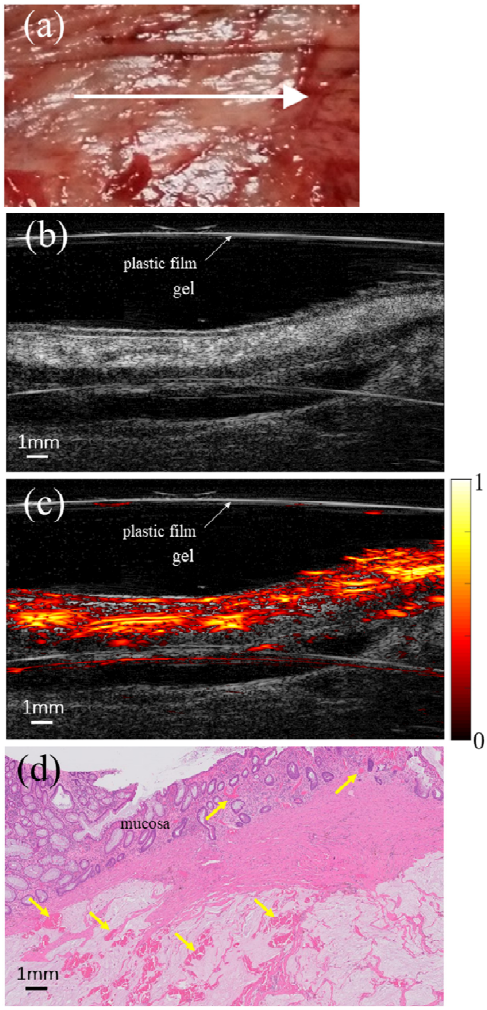

Fig. 7. Images of Specimen 4 – a rectal cancer treated with chemotherapy and radiation prior to surgical resection; histologic evaluation revealed no viable tumor in the specimen. (a) Photograph of the post treated rectum tumor area, (b) ultrasound image of the lesion area, (c) co-registered ultrasound and photoacoustic image; (d) H&E image, no residual tumor is found, blood vessels are identified by yellow arrows.

Biomedical Optics EXPRESS

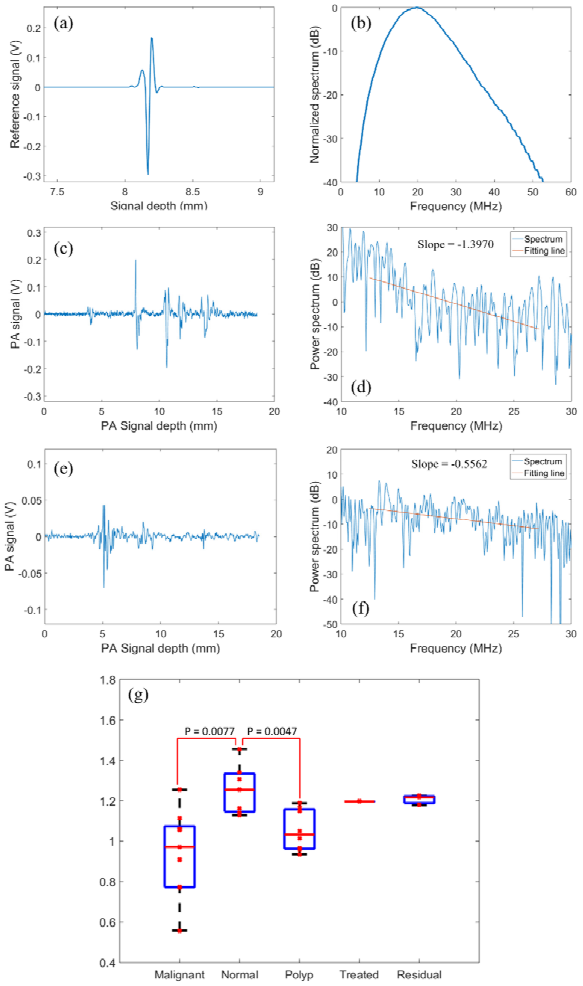

Fig. 8. (a) Ultrasound echo signal from glass; (b) fast Fourier transform of (a); (c) AR-PAM beam of normal tissue; (d) spectrum of (c); (e) AR-PAM beam of malignant tissue; (f) spectrum of (e); (g) Boxplot and P-value of photoacoustic spectrum slope (absolute value), including 4 malignant cases, 4 normal cases, 2 polyps cases, 1 treated case (rectal cancer with treatment) and 1 residual (colon cancer with treatment)

Table 2. Power spectrum slope value

	Colon cancer	Normal tissue	Polyp	Rectal lesion without residual disease	Colon tumor with residual disease
Average value per case	–1.1844	–1.2975	–1.0084	–1.1962	–1.2069
	–0.9392	–1.2518	–1.0805		
	–0.6642	–1.2174			
	–0.9628	–1.2537			
Mean value	–0.9376	–1.2551	–1.0444	–1.1962	–1.2069
Standard deviation	0.2131	0.0328	0.0510		

Biomedical Optics EXPRESS

4. Discussion

We report the initial design and testing of an acoustic resolution photoacoustic microscopy system on *ex vivo* human colon and rectum specimens. In addition to qualitatively describing the appearance of various histology when imaged with this system, we also report a method for quantitatively analyzing the different tissue profiles. Most importantly, these results suggest that AR-PAM may offer new discriminatory data to clinicians attempting to differentiate malignant from normal tissue in the human colon and rectum.

4.1. System performance

The AR-PAM system as described provides high resolution cross sectional photoacoustic and ultrasound imaging that also contains morphological data currently unavailable with traditional endoscopic or radiographic techniques. The system imaging head is designed as an endoscope for future human *in vivo* study. For current *ex vivo* sample study, forward viewing mode is used, however, for future *in vivo* endoscopic scanning of colon wall structures, the system can be operated in the side-viewing mode. The system resolution and penetration depth depend on the frequency of the ultrasound transducer. The system performance such as SNR was tested by imaging a black string inside calibrated intralipid solution at different depths of up to 4.5 mm, and the axial as well as lateral resolution were measured by imaging a carbon fiber. We obtained 18 to 42 dB SNR with a laser fluence well below the safety threshold, suggesting the ability to safely use this technology endoscopically in future *in vivo* patient study without averaging. Both lateral and axial resolutions are on the level of tens of microns, which is detailed enough to resolve colon wall structure and vasculature distribution. Blood vessels with a size smaller than the resolution, however, cannot be identified. Tissue penetration is about 8mm, which sufficiently images the submucosa and underlying muscle layer. Ultrasound imaging resolution and depth are on the same level as photoacoustic imaging. For both imaging modes, photoacoustic and ultrasound signal are detected directly without going through second medium, such as mirror or prism for redirecting the sound wave and introducing losses; therefore, maximum acoustic energy can be detected by the ultrasound transducer, which optimizes system signal-to-noise ratio.

4.2. Tissue characterization and differentiation

AR-PAM demonstrated the potential to differentiate benign from malignant tissue types in this pilot study. Though the study population was limited, clear trends appear within our data. Qualitatively, malignancies appear associated with disrupted layering of the bowel wall and a paucity of photoacoustic signal within the tumor itself. Polyps also show less blood vessels within the masses and in surrounding tissue when compared to cancers, and the photoacoustic signal from polyps are weaker than cancer. This phenomenon may be due to hypermetabolic activity of cancers compared to polypoid lesions. As a result, cancers require higher vascular flow than polyps to support their growth, leading to more pronounced PAM signal. Quantitatively, the imaged cancers are also associated with spectral slopes less than 1, which even in this small sample varies significantly from normal tissue. These differences appear due to changes in both the architecture and vascularity of tumors which, even at early stages, appear detectable by AR-PAM.

Interestingly, the changes observed in malignant tissue organization and vascularity may return to normal in the setting of significant response to chemotherapy and radiation. While the rectal tumor bed images from this study were collected after therapy – and thus lack baseline measurements for comparison, our findings suggest that treated lesions may regain normal layering and organized submucosal vasculature. Therefore, AR-PAM may be able to detect a complete response to medical therapy among rectal tumors – fulfilling a clinical need that current endoscopic and radiographic techniques cannot accomplish.

Biomedical Optics EXPRESS

Ultimately, the clinical utility of this instrument lies in its ability to identify small foci of cancer to facilitate early diagnosis or new malignancy or incomplete response to chemotherapy and radiation. The inability to identify incomplete responders, for example, is the main inhibitor to widespread adoption of nonoperative management of rectal cancer, a truly breakthrough option which will revolutionize rectal cancer care. Based on these preliminary results, AR-PAM may be the solution that increases cancer detection rates while sparing patients from highly morbid surgery overall.

4.3. Limitations

This small pilot study has limitations. First, the study included a small number of specimens. While the patterns described above appear consistent across multiple specimens, these findings need to be further validated with a larger patient pool and *in vivo*.

Second, the imaging speed is limited by the speed of the Ti:Sapphire laser (15Hz). In future, we plan to upgrade the laser system to kHz repetition rate, which can be used for *in vivo* patient studies.

5. Summary

Unlike existent technologies such as MRI, endorectal ultrasound, or white light endoscopy, AR-PAM appears to produce high resolution morphologic imaging that may assist in the detection of microscopic tissue clusters in the future. Initial data from *ex vivo* human colorectal tissue have demonstrated the feasibility of identifying colorectal cancer imaging features using a co-registered ultrasound and acoustic-resolution photoacoustic microscopy system. For malignant colorectal tissue, the cross-sectional structure is highly disorganized with central darkening of the photoacoustic signal inside the tumor. Quantitative analysis of photoacoustic spectral slope has demonstrated more high-frequency components in malignant tissue as compared to the normal colon tissue, which may be caused by significantly increased microvessel networks. For treated colorectal cancers, AR-PAM may identify completely responded lesions, which would significantly change surgical practice for these diseases.

Funding

National Institutes of Health (R01CA151570 (QZ)); the Washington University School of Medicine Surgical Oncology Basic Science and Translational Research Training Program (T32CA009621 (WC)).

Acknowledgments

We gratefully acknowledge the support of Michelle Sperry and June Smith for coordinating the patient enrollment for this study.

Disclosures

The authors declare that there are no conflicts of interest related to this article.

References

1. L. V. Wang and S. Hu, "Photoacoustic tomography: in vivo imaging from organelles to organs," Science **335**(6075), 1458–1462 (2012).
2. M. Xu and L. V. Wang, "Photoacoustic imaging in biomedicine," Rev. Sci. Instrum. **77**(4), 041101 (2006).
3. J. Laufer, P. Johnson, E. Zhang, B. Treeby, B. Cox, B. Pedley, and P. Beard, "In vivo preclinical photoacoustic imaging of tumor vasculature development and therapy," J. Biomed. Opt. **17**(5), 056016 (2012).
4. S. Hu and L. V. Wang, "Photoacoustic imaging and characterization of the microvasculature," J. Biomed. Opt. **15**(1), 011101 (2010).
5. J. Yao and L. V. Wang, "Photoacoustic Microscopy," Laser Photonics Rev. **7**(5), 758–778 (2013).
6. M. Xu and L. V. Wang, "Photoacoustic imaging in biomedicine," Rev. Sci. Instrum. **77**(4), 041101 (2006).

Biomedical Optics EXPRESS

7. J.-M. Yang, C. Favazza, R. Chen, J. Yao, X. Cai, K. Maslov, Q. Zhou, K. K. Shung, and L. V. Wang, "Simultaneous functional photoacoustic and ultrasonic endoscopy of internal organs in vivo," Nat. Med. **18**(8), 1297–1302 (2012).
8. J.-M. Yang, C. Li, R. Chen, B. Rao, J. Yao, C.-H. Yeh, A. Danielli, K. Maslov, Q. Zhou, K. K. Shung, and L. V. Wang, "Optical-resolution photoacoustic endomicroscopy in vivo," Biomed. Opt. Express **6**(3), 918–932 (2015).
9. E. M. Strohm and E .S. L. Berndl, and M. C. Kolios, "Probing red blood cell morphology using high-frequency photoacoustic," Biophys. J. **105**(1), 59 (2013).
10. G. Xu, Z.-X. Meng, J. D. Lin, J. Yuan, P. L. Carson, B. Joshi, and X. Wang, "The functional pitch of an organ: quantification of tissue texture with photoacoustic spectrum analysis," Radiology **271**(1), 248–254 (2014).
11. P. V. Chitnis, J. Mamou, and E. J. Feleppa, "Spectrum analysis of photoacoustic signals for characterizing lymph nodes," J. Acoust. Soc. Am. **135**(4), 2372 (2014).
12. H. Li, P. Kumavor, U. Salman Alqasemi, and Q. Zhu, "Utilizing spatial and spectral features of photoacoustic imaging for ovarian cancer detection and diagnosis," J. Biomed. Opt. **20**(1), 016002 (2015).
13. H. S. Salehi, H. Li, A. Merkulov, P. D. Kumavor, H. Vavadi, M. Sanders, A. Kueck, M. A. Brewer, and Q. Zhu, "Coregistered photoacoustic and ultrasound imaging and classification of ovarian cancer: ex vivo and in vivo studies," J. Biomed. Opt. **21**(4), 46006 (2016).
14. R. L. Siegel, K. D. Miller, S. A. Fedewa, D. J. Ahnen, R. G. S. Meester, A. Barzi, and A. Jemal, "Colorectal cancer statistics, 2017," CA Cancer J. Clin. **67**(3), 177–193 (2017).
15. S. P. Hiotis, S. M. Weber, A. M. Cohen, B. D. Minsky, P. B. Paty, J. G. Guillem, R. Wagman, L. B. Saltz, and W. D. Wong, "Assessing the predictive value of clinical complete response to neoadjuvant therapy for rectal cancer: an analysis of 488 patients," J. Am. Coll. Surg. **194**(2), 131–135 (2002).
16. American National Standards Institute, "American National Standard for the Safe Use of Lasers," ANSI Standard Z136.1 (American National Standards Institute, New York, 2000).